Novelty Journals

ISSN 2394-9651

International Journal of Novel Research in Physics Chemistry & Mathematics
Vol. 12, Issue 3, pp: (8-28), Month: September - December 2025, Available at: www.noveltyjournals.com

Boundary Condition Formulation and Validation in Finite Volume Modelling of Nano-Enhanced Phase Change Materials

Florence Awuor Misawo[*1], Onyango T. T. Mboya[2], Fredrick O. Nyamwala[1]

[1]Department of Mathematics, School of Biological &; Physical Sciences, Moi University, Eldoret, Kenya.

[2]Department of Pure and Applied Mathematics, Technical University of Kenya, Kenya.

DOI: https://doi.org/10.5281/zenodo.17710716

Published Date: 25-November-2025

Abstract: **Nano-Enhanced Phase Change Materials (NePCMs) have become high-performance thermal energy storage media as a result of their augmented thermal conductivity and faster melting–solidification behaviour. However, despite a great development in numerical modelling on NePCMs, one important methodological problem is still unknown: the formulation, implementation and validation of boundary conditions in Finite Volume Method (FVM) based simulations for a systematic way. This gap has helped to feed numerical instability, inaccurate melt-front prediction, and unreliable thermal-fluids behaviour in past studies. The present study overcomes this limitation by merging and validating a complete boundary condition in the form of a Neumann, Dirichlet and Mixed formulation in control volume discretisation. Using coupled momentum and energy equations, nanoparticle enhanced thermophysical models and matrix inversion schemes, the simulations were run for x- and y- direction momentum carrying as well as heat distribution. The results have shown that the specification of proper boundary conditions is an important factor in heat-flux continuity, velocity-field development, thermal stratification and numerical stability. The model captures realistic buoyancy-driven convection, uniform heat diffusion and stable temperature gradients. The study concludes that boundary-condition modelling is very basic in correct NePCM simulations. Policy and future recommendations involve the use of validated numerical frameworks in thermal-storage system designs, expansion of the model to transient, 3D problems, and inclusion of experimental benchmarking for improved predictive reliability.**

Keywords: **Boundary Condition Modelling, Finite Volume Method, Heat Transfer and Energy Storage, Nano-Enhanced Phase Change Materials, Numerical Stability Analysis, Thermophysical Property Enhancement.**

I. INTRODUCTION

A. Background Information

The demand for an effective thermal management in energy, building, transportation and electronics sectors developed intensively research into Phase Change Materials (PCMs) and recently Nano-Enhanced Phase Change Materials (NePCMs) due to enhanced thermal conductivity, uniform thermal storage performance and faster melting-solidification rates [13]. Driven by the global sustainability initiatives, as well as the needs of high-performance energy storage, the global PCM market, valued at USD 2.19 billion in 2025, is expected to reach USD 4.24 billion in 2029, at 18% CAGR with buildings alone having the potential to offset 25% of energy consumption with the advanced integration of PCMs. These trends put in evidence the growing need for appropriate modelling techniques which can predict the thermal behaviour of NePCMs in various operating conditions.

Due to this demand, some numerical studies have been devoted to the modelling for PCM and NePCM melting and solidification. Finite Volume Method (FVM)-based simulations have been able to find the broadest application due to its rigid adherence to the conservation principles. For example, cyclic melting and solidification of PCM/NePCM heat sinks by [16] by using the enthalpy-based FVM and the importance of proper enthalpy–temperature couplings and mushy zone modelling has been demonstrated by [1]. Additional studies which considered enhancement in heat transfer by fins and geometrical modifications indicate the complexity of the convection-conduction interactions in PCM systems [4]. Complementing these efforts, investigations connected to stability including [12] indicate that NePCM simulations are extremely sensitive to nanoparticles concentration, grid resolution, and thermal diffusivity.

Despite all these progresses, there is still a critical methodological gap with regard to formulation and validation of boundary conditions for FVM-based NePCM simulations. Guidance by boundary conditions are very much influenced to heat-flux continuity, velocity damping at phase-front as well as overall energy conservation, however, boundary conditions have been mostly applied in previous studies without proper evaluation or comparison between cases. This is an important omission as faulty boundary specifications may cause unstable simulations, invalid predictions of the interface and unreliable system level design choices. Therefore the task of this research is to formulate, classify and validate the boundary conditions formulations in the light of finite volume framework for NePCMs. By verification of Neumann, Dirichlet and mixed boundary conditions in representative geometries and comparison of results with analytical, numerical and experimental values published in literature, the research aims at providing a reliable and transferable framework for boundary conditions in order to improve its predictive powers and contribute to the optimized design of NePCM-based thermal energy systems.

B. Contribution

This study offers several original and technically significant contributions to numerical modelling of NePCMs, addressing long-standing limitations in existing literature. It establishes a systematic and mathematically rigorous framework for formulating, discretising and validating boundary conditions, including Neumann, Dirichlet and mixed types, within finite volume simulations of NePCM systems. Earlier studies generally adopted generic or untested boundary assumptions, which often resulted in numerical instability and inaccurate melt-front predictions; the present work resolves this gap by linking boundary specification directly to conservation laws and control volume flux balances. The study further introduces a fully coupled momentum energy inversion scheme capable of producing stable solutions of velocity and temperature fields under multiple boundary scenarios using tridiagonal matrix formulations and Gaussian inversion. This represents a methodological advancement over the single-equation or semi-coupled approaches commonly used in PCM modelling.

A validated finite-volume boundary-condition model is also presented, with its accuracy demonstrated through comparison with analytical Laplace solutions and physically consistent simulation outputs, an essential verification step that is often omitted in NePCM research. In addition, nanoparticle-dependent transport properties such as thermal conductivity, viscosity, heat capacity and latent heat are incorporated directly into the boundary-condition formulation, establishing a clear link between nanoparticle physics and boundary-driven heat-transfer behaviour, a relationship not captured in existing PCM or NePCM studies. The resulting framework is generalisable and extensible to transient, three-dimensional and experimentally benchmarked systems, thereby providing a robust foundation for the improved design and optimisation of advanced thermal-energy storage technologies.

II. RELATED WORKS

A. Existing Studies

[16] examined the difficulty of predicting melting and solidification behaviour in PCM and NePCM heat sinks where thermal response is strongly dependent on the nanoparticle concentration and boundary conditions of heat fluxes. Their study used an enthalpy-based finite volume method to simulate cyclic thermal loading and controlled nanoparticle dispersions for examination of conductivity enhancement. Numerical discretization was done on a fixed grid and boundary conditions were applied uniformly without case specific testing. Their results supported by the rapid melting rate and thermal uniformity enhancing with the increasing fraction of nanoparticles. They concluded that NePCMs have better heat sink performance. However, the effect of various boundary condition types was not included in the study, nor the stability, accuracy or conservation behaviour. The absence of analysis of the boundary conditions limits the applicability of their results over geometries and operating conditions. This neglect provides the motivation to the proposed study for the explicit testing, comparison and validation of boundary conditions within a finite volume scheme for NePCM simulations.

[1] capture mushy-zone behaviour and enthalpy-enthalpy-temperature coupling in PCM melting taking into account the numerical instability in case of incorrect boundary treatments. The method used to analyse transient melting under different thermal loadings was a hybrid of the Lattice Boltzmann and Finite Volume methods. Using complex enthalpy modelling and grid refinement the method refined the resolution of the phase front while using general thermal boundary conditions. Results showed improved accuracy of studying the melt front evolution and improved coupling between latent heat and the temperature fields. While the work was a step forward in the development of PCM modelling, it did not consider the role of boundary conditions in the flux continuity and stability in the presence of nanoparticles. No systematic testing and comparison of Neumann, Dirichlet or mixed boundaries were carried out and effects of nanoparticles were not considered. These omissions confine generalization to NePCM systems. This gap reinforces the need of current study which focuses on boundry condition formulation and validation on NePCM heat transfer models.

[4] studied the poor heat transfer capability of conventional PCMs by focusing on the slow solidification as a result of low thermal conductivity. Their study involved the use of a two dimension finite volume model and enthalpy-porosity method to redesign fin arrangements in a triplex tube heat exchanger. Simulations were used to evaluate the effect of modified fin geometries on heat transfer and solidification time. Findings showed that the placement of fins strategically can reduce solidification time by more than 20%, which results in the improvement of thermal systems efficiency. Although the study showed good improvement of heat transfer intensity, it focused mainly on the optimisation of geometry and did not solve the numerical problems such as the formulation of boundary conditions, stability, and accuracy under NePCM conditions. The effect of the boundary conditions on the local distribution and convergence of heat flux were not analyzed. The lack of evaluation of boundary conditions restricts extrapolation to NePCM modelling, for which boundary behaviour is strongly influence on the phase front tracking. This gap underlines the need for the proposed research which systematically investigates and validates boundary conditions in the framework of the finite volume NePCM.

[12] discussed the issue of numerical instability of NePCM simulations, which is due to the nanoparticle induced effects in thermal diffusivity, leading to a high sensitivity of any NePCM simulation to the selection of grid size and time step. The study obtained discretized energy equations based on control volume method and formulated stability conditions by using Courant number method. MATLAB simulations produced phase plane maps of stability changing as the concentration of nanoparticles and the fineness of the grid increased. Although this work led to a great advance in understanding the stability behaviour, the effect of boundary conditions on numerical instability was not examined. Boundary conditions were assumed and not tested and comparison of Neumann, Dirichlet or mixed boundaries was not considered. Because the treatment of boundaries has significant impacts on both heat flux continuity and convergence in the finite volume models, the omission of the boundary treatment is an important overshadowing gap. This motivates the present study which extends the previous works by developing, analyzing and validating boundary conditions for a reliable NePCM simulation.

B. Research Gap

Table 1: Literature Gap Matrix for Boundary-Condition Modelling in NePCMs

Study	Key Focus	Critique	Gaps
[16]	Modelled PCM/NePCM melting using enthalpy-based FVM under cyclic heating.	Boundary conditions applied generically without evaluation.	No analysis of BC influence or comparison across BC types.
[1]	Developed hybrid LB–FVM scheme for PCM melting with mushy-zone modelling.	Did not assess BC effects; no NePCM consideration.	Missing boundary-condition validation for NePCM simulations.
[4]	Optimized fin arrangements using 2D FVM for PCM solidification enhancement.	Focused on geometry, not numerical boundary formulation.	Unclear BC impact on heat flux and phase-front prediction.
[12]	Studied NePCM stability using control-volume discretization and phase-plane analysis.	Stability analysed without testing boundary-condition roles.	Need to evaluate BC contributions to numerical stability.
Synthesis of Gaps	—	—	Literature lacks systematic formulation, comparison, and validation of boundary conditions in FVM NePCM modelling.

Novelty Journals

ISSN 2394-9651

International Journal of Novel Research in Physics Chemistry & Mathematics
Vol. 12, Issue 3, pp: (8-28), Month: September - December 2025, Available at: www.noveltyjournals.com

III. RESEARCH METHODOLOGY

A. PCM Physical Model

The physical model representing PCM under consideration is enclosed within an annular cavity formed between two concentric horizontal cylindrical shells with the inner wall considered to be very thin and subjected to a constant heat of 235 ^{0}C (1^oC higher than the melting point of the PCM) at Γ_1. The walls Γ_2, Γ_3 and Γ_4 are under adiabatic conditions, enclosing the domain within which simulation of storing of thermal energy takes place during charging. The source of heat triggers melting of the PCM causing it to move upwards within the domain at an initial velocity of 0.03 m/s. Elementary cross-section of the domain within x and y, is illustrated in Figure 1.

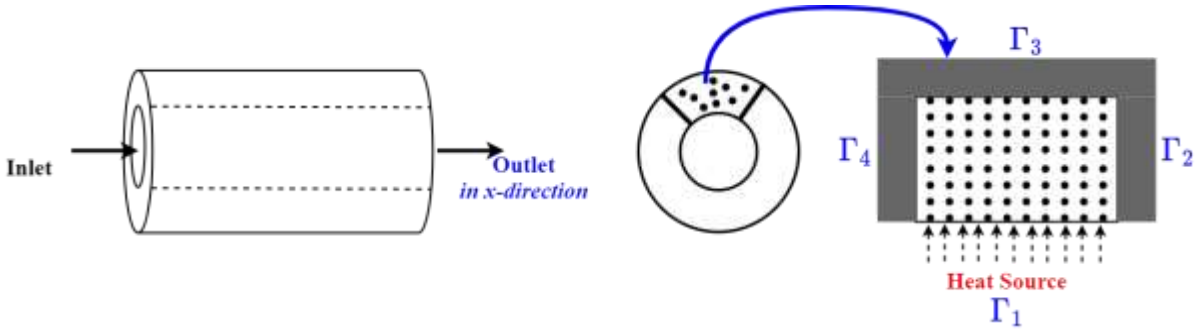

Figure 1: Cross-sectional cavity for modelling the phase change process. The length of the boundaries (x and y) enclosing the domain are in the ratio $1:1$ and the boundary conditions are presented in Figure 2.

B. Governing Equations

Considering Nano fluid as a continuous media with thermal equilibrium between the base fluid and the solid nanoparticles, the governing equations are derived based on the fact that the dynamical behavior of a fluid is determined by coupling conservation laws of mass, momentum and energy.

1) Conservation of mass

Conservation equation for mass or continuity equation, for a control volume states that the rate of change of the mass inside the control volume V is equal to the difference between inflow and outflow mass fluxes across a volume surface S, given as;

$$\frac{\partial \rho}{\partial t} + \nabla \cdot (\rho \vec{V}) = 0 \tag{1}$$

where ρ is the fluid density and $\vec{V}$ is the fluid velocity vector. Due to incompressibility of the fluid flow after melting process, $\frac{\partial \rho}{\partial t}$ reduces to zero since the density is assumed to be constant and hence the equation becomes

$$\nabla \cdot \vec{V} = 0 \tag{2}$$

However, for problems with moving grids, which involve continuous changes of control volume, this term might be considered depending on the numerical method employed.

2) Momentum Equations

A second set of equations can be derived by applying Newton's Second Law of motion to find the relationship between the forces on the patch of fluid and the acceleration of the fluid. Conservation equation for momentum states that the total variation of momentum, represented by the time variation of momentum within the control volume and the transfer of momentum across the boundary of the control volume by fluid motion (called convection or advection) is caused by the net force acting on the fluid in the control volume, defined as

$$\rho[\frac{\partial \vec{U}}{\partial t} + \frac{\partial \vec{V}}{\partial t} + (\vec{V} \cdot \nabla)\vec{V}] = -\nabla p + \mu \nabla^2 \vec{U} + \mu \nabla^2 \vec{V} + \rho \vec{g}(T - T_0) + S, \tag{3}$$

Novelty Journals

ISSN 2394-9651

International Journal of Novel Research in Physics Chemistry & Mathematics
Vol. 12, Issue 3, pp: (8-28), Month: September - December 2025, Available at: www.noveltyjournals.com

The momentum equation in x direction is given by

$$\rho\left(\frac{\partial u}{\partial t}+u\frac{\partial u}{\partial x}+v\frac{\partial u}{\partial y}\right)=-\frac{\partial p}{\partial x}+\mu\left(\frac{\partial^2 u}{\partial x^2}+\frac{\partial^2 u}{\partial y^2}\right), \tag{4}$$

and momentum equation in y direction

$$\rho(\frac{\partial v}{\partial t}+u\frac{\partial v}{\partial x}+v\frac{\partial v}{\partial y})=-\frac{\partial p}{\partial y}+\mu(\frac{\partial^2 v}{\partial x^2}+\frac{\partial^2 v}{\partial y^2})+\beta\rho g(T-T_r) \tag{5}$$

where ρ is the density, p is the pressure,μ is the dynamic viscosity, t is the time, β is the thermal expansion coefficient of the PCM, g is the gravitational accelation, T is the temperature, T_r is the reference temperature. Assumptions to be made in phase change process are: the liquid phase of PCM is Newtonian and laminar, incompressible fluid with transient state of flow, all thermophysical properties of the PCM are assumed to be constant, the Boussinesq model is used in the buoyancy force term. In the energy equations, the internal heat generation and the viscous dissipation effect are neglected. The pressure inside the domain is constant and hence $\frac{\partial P}{\partial y}$ and $\frac{\partial P}{\partial x}$ reduce to 0 leaving the momentum equations in x and y direction as:

$$\rho(\frac{\partial u}{\partial t}+u\frac{\partial u}{\partial x}+v\frac{\partial u}{\partial y})=\mu(\frac{\partial^2 u}{\partial x^2}+\frac{\partial^2 u}{\partial y^2}) \tag{6}$$

with the boundary condition imposed on the x-axis as

$$On \qquad \Gamma_1=\{0,1\}\times\{0\},\frac{\partial T}{\partial n}=g(T)$$

$$On \qquad \Gamma_3=\{1\}\times\{0,d\},\frac{\partial T}{\partial n}=0$$

$$\rho(\frac{\partial v}{\partial t}+u\frac{\partial v}{\partial x}+v\frac{\partial v}{\partial y})=\mu(\frac{\partial^2 v}{\partial x^2}+\frac{\partial^2 v}{\partial y^2})+\beta\rho g(T-T_r) \tag{7}$$

Boundary conditions in y-axis direction equation is give as:

$$On \qquad \Gamma_2=\{1\}\times\{0,d\}, \qquad \frac{\partial T}{\partial n}=0$$

$$On \qquad \Gamma_4=\{0\}\times\{0,d\}, \qquad \frac{\partial T}{\partial n}=0$$

3) Energy Equation

In fluid flow rate of increase in energy of the fluid particles is equal to the sum of net rate of energy gained by fluid particles and net rate of work done on the particles, given below as:

$$\frac{\partial(\rho H)}{\partial t}+\rho c_p[u\frac{\partial T}{\partial x}+v\frac{\partial T}{\partial y}]=k[\frac{\partial^2 T}{\partial x^2}+\frac{\partial^2 T}{\partial y^2}] \tag{8}$$

The underlying principle upon which the energy equation is derived, is the first law of thermodynamics. It states that any changes in time of the total energy inside control volume are caused by the rate of work of forces acting on the volume and by the net heat flux into it. Boundary condition for energy equation in Eqn. (8) is given by

Novelty Journals

ISSN 2394-9651

International Journal of Novel Research in Physics Chemistry & Mathematics
Vol. 12, Issue 3, pp: (8-28), Month: September - December 2025, Available at: www.noveltyjournals.com

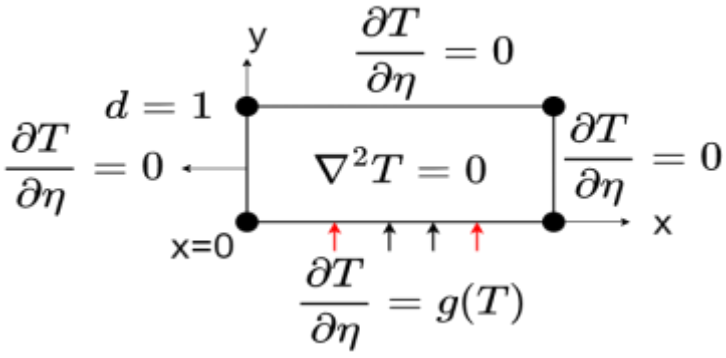

Figure 2: Illustration of the Boundary Condition for the energy equation.

C. Non-dimensionlization and Discretisation of the governing equations

Non-dimensionlisation is the partial or full removal of physical dimensions from an equation involving physical quantities by a suitable substitution of variables. Reynold Number being one of the dimensionless number gives a measure of the ratio of inertia(resistant to change or motion) forces to viscous forces. Laminar flows occurs at low Reynolds's Number whereas turbulent flow occurs at high Reynold's number. The following variables are used to non dimensionlize the parameters: time, distance, velocity, temperature and pressure as:

$$t^* = \frac{t}{L/U_\infty},\ x^* = \frac{x}{L},\ y^* = \frac{y}{L},\ z^* = \frac{z}{L},\ u^* = \frac{u}{U_\infty},\ v^* = \frac{v}{U_\infty},\ w^* = \frac{w}{U_\infty},\ p^* = \frac{p-p_\infty}{\rho/U_\infty^2},\ T^* = \frac{T-T_\infty}{\Delta T}, T = T^* \triangle T + T_\infty$$

Discretization of governing equations follows three steps namely domain discretization, time discretization and governing equations discretization. Domain discretization involves numerical partition of the grid, which replaces the continuous space with a finite number of discrete elements with computational points at their centroids. At these points, solution of dependent variables are computed. This process is termed as grid generation. Time discretization assumes division of the entire time interval into a finite number of small subintervals, called time steps with guarantee convergence of the solution.

1) Non dimensionlisation and Discretiastion of Conservation of Mass Equation

The flow of molten PCM is governed by continuity equation and momentum equations expressed in cartesian coordinates. Non dimesionlising Equation (1), yields

$$\triangle y^*(u^*_{i+1} - u^*_{i-1}) + \triangle x^*(v^*_{j+1} - v^*_{j-1}) = 0 \tag{9}$$

2) Non-dimesionlization of Momentum equations

Non-dimensionlizing Equation (4), momentum equation in x-direction using, the non-dimensionalization variables, we get

$$\left(\frac{\partial u^*}{\partial t^*} + u^*\frac{\partial u^*}{\partial x^*} + v^*\frac{\partial u^*}{\partial y^*}\right) - \frac{\mu}{\rho L U_\infty}\left(\frac{\partial^2 u^*}{\partial x^{*2}} + \frac{\partial^2 u^*}{\partial y^{*2}}\right) = 0 \tag{10}$$

resulting into Non-dimensionlised momentum equation in x direction with Reynolds number $\frac{\mu}{\rho L U_\infty} = \frac{1}{Re},\ Re = \frac{\rho L U_\infty}{\mu}$

3) Discretisation of Momentum equations in X direction

Integrating Equation (10) in the control volume at the central node, P in Figure 5, yields

$$\begin{aligned} &C[u_{k+1} - u_k] + 0.5A\bar{u}_i(u_{(i+1)} - u_{(i-1)}) + 0.5B\bar{v}_j(u_{(j+1)} - u_{(j-1)}) \\ &-\frac{\mu_{nf}}{\rho_{nf} L U_\infty}\{Q(u_{i+1} - 2u_i + u_{i-1}) + R'(u_{j+1} - 2u_j + u_{j-1})\} = 0 \end{aligned} \tag{11}$$

With the presence of nanoparticles and the assumption that they are spherical in shape to guarantee the validity of the Brinkman model and the maxwell model for heat transfer, we compute the effective viscousity of NEPCMs using Brinkman model as follows,

Novelty Journals

ISSN 2394-9651

International Journal of Novel Research in Physics Chemistry & Mathematics
Vol. 12, Issue 3, pp: (8-28), Month: September - December 2025, Available at: www.noveltyjournals.com

$$\mu_{nf} = \frac{\mu_{PCM}}{(1-\phi)^{2.5}} \tag{12}$$

where ϕ is the volume fraction of nanoparticles, μ_{PCM} is the dynamic viscosity of pure PCM, and μ_{nf} is the dynamic viscosity of NEPCMs.

4) Non dimensionlization of Momentum Equations in y direction

Non dimensionlizing Equation (5), momentum equation in y-direction using the non dimensionalization variables results in:

$$\left(\frac{\partial v^*}{\partial t^*} + u^*\frac{\partial v^*}{\partial x^*} + v^*\frac{\partial v^*}{\partial y^*}\right) - \frac{\mu}{\rho L U_\infty}\left(\frac{\partial^2 v^*}{\partial x^{*2}} + \frac{\partial^2 v^*}{\partial y^{*2}}\right) - \frac{L}{U_\infty^2}\beta g(T^* \triangle T + T_\infty - T_r) = 0 \tag{13}$$

5) Discretisation of Momentum Equations in y direction

Integrating Equation (13) in the control volume at node $P(i,j)$ in Figure 5, yields

$$\begin{aligned} &C[(v_{(k+1))} - (v_{(k)})] + 0.5Au_i(v_{(i+1)} - v_{(i-1)}) + 0.5Bv_j(v_{(j+1)} - v_{(j-1)}) \\ &= \frac{1}{Re}\{Q(v_{i+1} - 2v_i + v_{i-1}) + R'(v_{j+1} - 2v_j + v_{j-1})\} + D\{\frac{L}{U_\infty^2}\beta g((T \triangle T + T_\infty) - T_r)\} \end{aligned} \tag{14}$$

6) Non Dimesionlisation and Discretisation of Conservation of Energy Equation

Refer to Conservation of energy Equation (8), the enthalpy H of PCMs is defined as,

$$H = C_p(T - T_r) + f_l L \tag{15}$$

where f_l is the PCM liquid fraction and L is the latent heat of the PCMs. By caculating the enthalpy H of PCMs, the liquid fraction and temperature can be updated by the following equations

$$f_1 = \begin{cases} 0, & H \le H_s \\ \frac{H - H_s}{H_l - H_s}, & H_s \le H < H_l \\ 1, & H \ge H_l \end{cases} \tag{16}$$

$$T = \begin{cases} T = \frac{H_s - H}{c_p}, & H \le H_s \\ T_m, & H_s < H < H \\ T + \frac{H_s - H}{c_p}, & H \le H_l \end{cases} \tag{17}$$

7) Non-dimensionlisation of Conservation of Energy Equation

Non-dimensionalizing Equation (8) using the non-dimensionalization variables, yields,

$$\begin{aligned} &\frac{U_\infty}{L}\frac{\partial(\rho H)}{\partial t^*} + \rho C_p[u^*\frac{U_\infty}{L}\frac{\partial(T^*\triangle T + T_\infty)}{\partial x^*} + v^*\frac{U_\infty}{L}\frac{(T^*\triangle T + T_\infty)}{\partial y^*}] \\ &= \frac{k}{L}[\frac{\partial^2(T^*\triangle T + T_\infty)}{\partial x^{*2}} + \frac{\partial^2(T^*\triangle T + T_\infty)}{\partial y^{*2}}] \end{aligned} \tag{18}$$

Multiplying Equation (18) by $\frac{L}{U_{infty}}$ and taking $T_\infty = 0$, yields

$$\frac{\partial(\rho H)}{\partial t^*} + \rho C_p[u^*\frac{\partial(T^*\triangle T)}{\partial x^*} + v^*\frac{\partial(T^*\triangle T)}{\partial y^*}] = \frac{k}{U_\infty}[\frac{\partial^2(T^*\triangle T)}{\partial x^{*2}} + \frac{\partial^2(T^*\triangle T)}{\partial y^{*2})}] \tag{19}$$

Further simplification of Equation (19) as we multiply by $\frac{1}{\triangle T}$ yields,

$$\frac{1}{\triangle T}\frac{\partial(\rho H)}{\partial t^*} + \rho C_p[u^*\frac{\partial T^*}{\partial x^*} + v^*\frac{\partial T^*}{\partial y^*}] = \frac{k}{U_\infty}[\frac{\partial^2 T^*}{\partial x^{*2}} + \frac{\partial^2 T^*}{\partial y^{*2}}] \tag{20}$$

Novelty Journals

ISSN 2394-9651

International Journal of Novel Research in Physics Chemistry & Mathematics
Vol. 12, Issue 3, pp: (8-28), Month: September - December 2025, Available at: www.noveltyjournals.com

8) Discretisation of Conservation of Energy Equations

Discretizing conservation of energy Equation (20) yields,

$$S\{H_{k+1} - H_k\} + 0.5A\rho(C_p)u_i^*(T^*_{(i+1)} - T^*_{(i-1)}) + 0.5B\rho(C_p)v_j^*(v^*_{(j+1)} - T^*_{(j-1)}) = \frac{k_{nf}}{U_\infty}\{Q(T^*_{i+1} - 2T_i^* + T^*_{i-1}) + R(T^*_{j+1} - 2T_j^* + T^*_{j-1})\} \quad (21)$$

where $S = \frac{\triangle x \triangle y}{\triangle T}$, the simplified discretised energy equation after dropping * yields,

$$S(H_{k+1} - H_k) + 0.5A\rho(C_p)u_i(T_{(i+1)} - T_{(i-1)}) + 0.5B\rho(C_p)v_j(T_{(j+1)} - T_{(j-1)}) = \frac{k_{nf}}{U_\infty}\{Q(T_{i+1} - 2T_i + T_{i-1}) + R'(T_{j+1} - 2T_j + T_{j-1})\} \quad (22)$$

The thermal conductivity of NEPCM is calculated according to the Maxwell model as

$$k_{nf} = k_{PCM}\frac{k_p + 2k_{PCM} - 2(k_{PCM} - k_p)\phi}{k_p + 2k_{PCM} + (k_{PCM} - k_p)\phi} \quad (23)$$

where k_{PCM}, k_p, and k_{nf} are thermal conductivities of pure PCMs, nanoparticles and NEPCMs respectively. The density of nanofluid ρ_{nf} is calculated as;

$$\rho_{nf} = (1 - \phi)\rho_{PCM} + \phi\rho_p \quad (24)$$

where ρ_{PCM}, and ρ_p are densities of pure PCM and nanoparticles. The heat capacitance of NEPCMs $(\rho c_p)_{nf}$ is defined as

$$(\rho c_p)_{nf} = (1 - \phi)(\rho c_p)_{PCM} + \phi(\rho c_p)_p \quad (25)$$

where $(\rho c_p)_{PCM}$ is the heat capacitance of the PCM, and $(\rho c_p)_p$ is the heat capacitance of nanoparticles. Thermal expansion volume of NEPCMs $(\rho\beta)_{nf}$ is given as

$$(\rho\beta)_{nf} = (1 - \phi)(\rho\beta)_{PCM} + \phi(\rho\beta)_p \quad (26)$$

where $(\rho\beta)_{PCM}$ and $(\rho\beta)_p$ are thermal expansion volume of pure PCM and nanoparticles, respectively. The latent heat of NEPCMs is computed as

$$(\rho L)_{nf} = (1 - \phi)(\rho L)_{PCM} \quad (27)$$

where $(\rho L)_{PCM}$ is the latent heat of pure PCM. Then the coresponding enthalpy of NEPCM H_{nf} is given as

$$H_{nf} = Cp_{nf}(T - T_r) + f_l L_{nf} \quad (28)$$

D. Control Volume

The control volume approach provides a rigorous and physically consistent framework for solving conservation–law-based problems in engineering. Its central principle is the enforcement of mass, momentum, and energy conservation within each discrete region of the domain. By subdividing the domain into finite control volumes and integrating the governing partial differential equations (PDEs) over each volume, the continuous equations are transformed into algebraic expressions suitable for numerical computation [17]. This makes the method particularly efficient for simulating heat transfer and fluid flow processes in complex geometries.

Figure 3 illustrates the systematic node numbering convention adopted for the finite element discretization. With N nodes along the vertical direction and M nodes horizontally, the mesh contains a total of MN nodes. Numbering proceeds column-wise: starting from the bottom-left node, progressing upward, and then moving to the next column on the right. Consequently, the rightmost boundary corresponds to nodes with indices $MN - N + 1$ to MN, simplifying their extraction for the implementation of Neumann boundary conditions. This structured arrangement also facilitates efficient assembly of global stiffness and mass matrices.

ISSN 2394-9651

International Journal of Novel Research in Physics Chemistry & Mathematics
Vol. 12, Issue 3, pp: (8-28), Month: September - December 2025, Available at: www.noveltyjournals.com

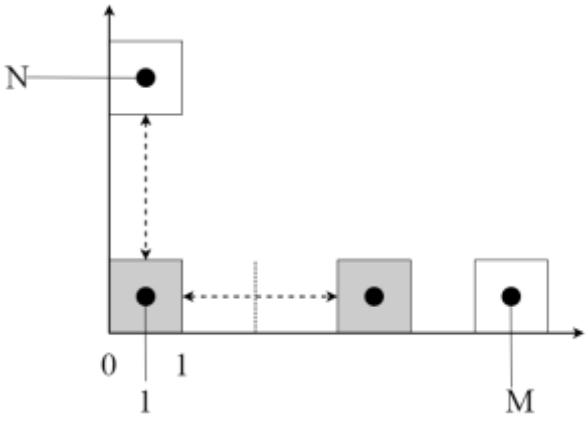

Fig. 3: Illustration of node numbering convention where $i = MN - M$ and $j = MM - N + 1, \dots, NM$.

A zoomed representation of the rightmost boundary is shown in Figure 4, identifying boundary regions categorized as Case I, II, and III, each associated with different boundary conditions represented in Eqs. (32), (35), and (38), respectively.

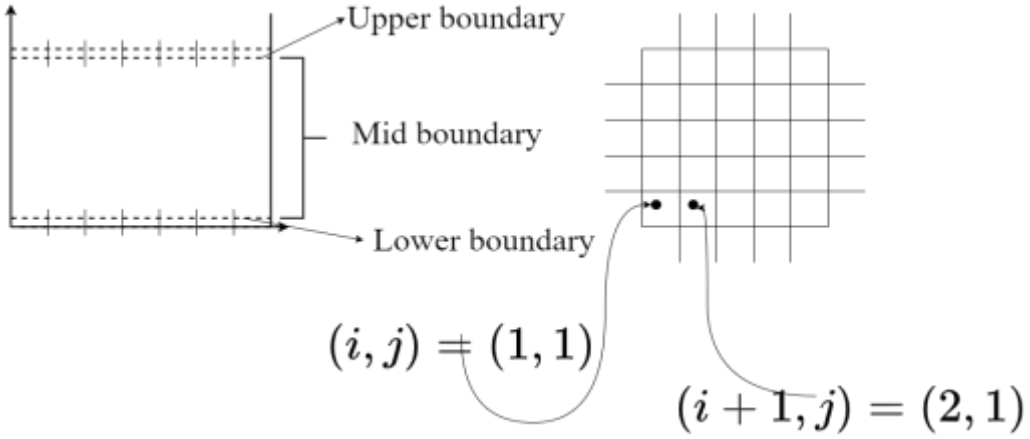

Figure 4: Focus boundaries for Case I, II and III.

In FVM, nodes are located at the geometric centers of control volumes, ensuring that conservation laws are satisfied over finite areas rather than at isolated points. The method evaluates fluxes across control-volume faces at each time step, and the discretization process replaces differential terms with algebraic relationships between neighboring nodes. This ensures local conservation of transported quantities and supports stable, physically meaningful solutions. A representative two-dimensional control volume is shown in Figure 5.

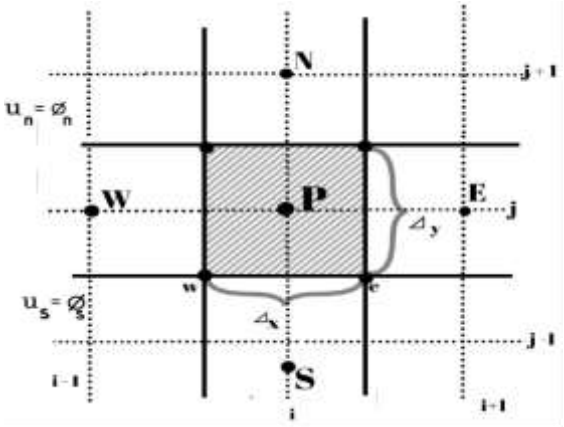

Figure 5: 2-dimensional control Volume

Novelty Journals

ISSN 2394-9651

International Journal of Novel Research in Physics Chemistry & Mathematics
Vol. 12, Issue 3, pp: (8-28), Month: September - December 2025, Available at: www.noveltyjournals.com

E. Inversion of the Heat Transfer and Heat Storage Problem

1) X-Direction Momentum

Considering Equations (11), (14) and (22) governing the physical process of steady coupled momentum, they can be converted into an equivalent system of linear equations involving velocities of the interface and its normal boundary values of velocities at all points on the boundary of its solution domain. By solving the system of linear algebraic equations using initial guesses in the discretised momentum equation then using the information obtained to solve the coupled energy Equation (8) to obtain uniquely approximate solution in the iterative process in the x and y direction respectively. The well posed problem can be solved using direct inversion schemes namely Gaussian methods for tri-diagonal schemes.

A regular bounded domain Ω represents the region occupied by the NePCM which contains heat source at the base moving at a speed of $0.03m/s$. Numerical approach becomes viable as solving the coupled equatons analytically results into ill possedness. The approach involves discretizing the domain in the x direction Γ_i for $i = 1, M$, on Eqn. (11) and y direction Γ_j on (14), for $j = 1, \dots, N$. This discretizes the domain Ω into nodes $\delta\Omega_{i,j}, i = j = 0,1, \dots, M, N,\ 0,1, \dots, M(M \times N)$, for $(M, N) = (10,10)$. With the center of the nodes varying from $1,2, \dots, M$ and $1,2, \dots, N$. For $\sum_{i=1}^{N}$, take $i = M \times N = NM$, number of central nodes. Dividing the region into 3 subdomain as follows:

$$\begin{aligned} j &= \overline{1, N} \\ j &= N+1, \dots, NM-N, \\ j &= NM-N+1, \dots, NM \end{aligned} \tag{29}$$

Discretizing the domain into three major subsection in the y-axis direction, lower boundary to have center nodes from $1, N$, mid section to have the nodes extending from $\bar{N}+1, \dots, NM-N$ and the upper boundary to have the center nodes. $\bar{N}M - N+1, \dots, NM$. The momemtum equation in the x-direction is then approximated as follows by system on NM algebraic tridiagonal system of equations. At the node, $\{i, j\} = \{1,1\}$ with the unknown values unknown values are $u_{1,1}$, $u_{2,1}$, From Eqn. (11) transforms to Eqn. (30):

$$\begin{aligned} &C[u_{k+1} - u_k] + 0.125A\{u_{(i+1)}\bar{u}_{(i+1)} + 2u_{(i+1)}\bar{u}_i - 2\bar{u}_{i-1}u_i - u_{(i-1)}\bar{u}_{(i-1)}\} \\ &+0.5B\bar{v}_j(u_{(j+1)} - u_{(j-1)}) \\ &-\frac{\mu_{nf}}{\rho_{nf}LU_\infty}\{Q(u_{i+1} - 3u_i + 2u_{i-1}) + R(u_{j+1} - 3u_j + 2u_{j-1})\} = 0 \end{aligned} \tag{30}$$

Since this is a steady case of heat energy transfer, $C(u_{k+1} - u_k)$ term reduces to 0 and letting $\frac{\mu_{nf}}{\rho_{nf}LU_\infty} = \frac{1}{Re}$ and collecting like terms such that the unknown terms ($u_{1,1}$ and $u_{2,1}$) remain on the left hand side of the equation, yields

$$\begin{aligned} &\{-0.25Au_{0,1} + \tfrac{3}{Re}\{Q + R'\}u_{1,1} \\ &+\{0.125A\bar{u}_{2,1} + 0.25A\bar{u}_{1,1} - \tfrac{1}{Re}Q\}u_{2,1} \\ &= 0.125A\bar{u}_{0,1}u_{0,1} - 0.5B\bar{v}_{1,1}u_{1,2} + 0.5B\bar{v}_{1,1}u_{1,0} + \tfrac{1}{Re}\{2Q + R(u_{1,2} + 2u_{1,0})\} \end{aligned} \tag{31}$$

Let the coefficient of $u_{1,1}$ be A_1, the coefficient of $u_{2,1}$ be A_2, the known values on the right hand side be d_1, yields equation

$$A_1u_{1,1} + A_2u_{2,1} = d_1 \tag{32}$$

At the node, i=2, $i = (NM - N)$, and j=1, unknown values are $u_{1,1}$, $u_{2,1}$ and $u_{3,1}$,

$$\begin{aligned} &C(u_{k+1} - u_i) + 0.125A\{\bar{u}_{3,1}u_{3,1} + 2u_{3,1}\bar{u}_{2,1} - 2\bar{u}_{1,1}u_{2,1} - u_{1,1}\bar{u}_{1,1}\} \\ &+0.5Bv_{2,1}(u_{2,2} - u_{2,0}) \\ &-\tfrac{1}{Re}\left(Q(u_{3,1} - 2u_{2,1} + u_{1,1}\right) + R\{u_{2,2} - 3u_{2,1} + 2u_{2,0}\} = 0 \end{aligned} \tag{33}$$

Since this is a steady case of heat energy transfer, $C(u_{k+1} - u_k)$ term reduces to 0. Letting $\frac{\mu_{nf}}{\rho_{nf}LU_\infty} = \frac{1}{Re}$ and collecting like terms such that the unknown terms ($u_{1,1}$, $u_{2,1}$) and $u_{3,1}$ are left on the left hand side of the equation, yields

$$\begin{aligned}&\sum_{i=N+1}^{NM-N}[\{-0.125A\bar{u}_{i+1,1}-\frac{1}{Re}Q\}u_{i,1}+\{-0.125A\bar{u}_{i,1}+\frac{1}{Re}(2Q+3R)\}u_{i+1,1}\\&+\{0.125A\bar{u}_{i+2,1}+0.25\bar{u}_{i+1,1}-\frac{1}{Re}Q\}u_{i+2,1}]+\\&0.5B\bar{v}_{2,1}(u_{i+1,2}-u_{i+1,0})-\frac{1}{Re}(R'(u_{i+1,2}+2u_{i+1,0})\end{aligned}\tag{34}$$

In index notation, Eqn. (34) becomes,

$$A_3u_{1,1}+A_4u_{2,1}+A_5u_{3,1}=d_2\tag{35}$$

At the node $i=10$ and $j=1$, Unknown values are $u_{9,1},\ u_{10,1}$

$$\begin{aligned}&0.125A(\bar{u}_{11,1}\bar{u}_{11,1}+2\bar{u}_{11,1}u_{10,1}-2\bar{u}_{9,1}u_{10,1}-\bar{u}_{9,1}u_{9,1})\\&+0.5B\bar{v}_{10,1}(u_{11,1}-u_{10,0})\\&-\frac{\mu_{nf}}{\rho_{nf}LU_\infty}\{Q(2u_{11,1}-3u_{10,1}+u_{9,1})+R'(u_{10,2}-3u_{10,1}+2u_{10,0})\}=0\end{aligned}\tag{36}$$

Since this is a steady case of heat energy transfer, $C(u_{k+1}-u_k)$ term reduces to 0 and collecting like terms in order to have unknown terms $u_{9,1},\ u_{10,1}$, on the left hand side of the equation and letting $\frac{\mu_{nf}}{\rho_{nf}LU_\infty}=\frac{1}{Re}$ yields,

$$\begin{aligned}&[\{-0.125A\bar{u}_{9,1}-\frac{Q}{Re}\}u_{9,1}+\\&\{0.25A\bar{u}_{11,1}-0.25A\bar{u}_{9,1}+\frac{3}{Re}(Q+R')\}u_{10,1}]\\&=-0.125A\bar{u}_{11,1}u_{11,1}-0.5B\bar{v}_{10,1}u_{11,1}+\bar{0}.5B\bar{v}^*_{10,1}u_{10,0}\\&+\frac{1}{Re}\{2Qu_{11,1}+R'(u_{10,2}+2u_{10,0})\end{aligned}\tag{37}$$

Let the coefficient of $u_{9,1}$ be A_{27} ,the coefficient of $u_{10,1}$ be A_{28} and the known values on the right hand side be d_{10}, yields equation

$$A_{27}u_{9,1}+A_{28}u_{10,1}=d_{10},\tag{38}$$

which can be further processed to form matrix Eqn. (39).

$$\begin{bmatrix}A_1&A_2&0&0&0&0&0&0&0&0\\A_3&A_4&A_5&0&0&0&0&0&0&0\\0&A_6&A_7&A_8&0&0&0&0&0&0\\0&0&A_9&A_{10}&A_{11}&0&0&0&0&0\\0&0&0&A_{12}&A_{13}&A_{14}&0&0&0&0\\0&0&0&0&A_{15}&A_{16}&A_{17}&0&0&0\\0&0&0&0&0&A_{18}&A_{19}&A_{20}&0&0\\0&0&0&0&0&0&A_{21}&A_{22}&A_{23}&0\\0&0&0&0&0&0&0&A_{24}&A_{25}&A_{26}\\0&0&0&0&0&0&0&0&A_{27}&A_{28}\end{bmatrix}\begin{bmatrix}u_1\\u_2\\u_3\\u_4\\u_5\\u_6\\u_7\\u_8\\u_9\\u_{10}\end{bmatrix}=\begin{bmatrix}d_1\\d_2\\d_3\\d_4\\d_5\\d_6\\d_7\\d_8\\d_9\\d_{10},\end{bmatrix}\tag{39}$$

where the coefficients are:

$$\begin{aligned}A_i&=0.25A(u_{i+1}-u_{i-1})+\frac{3Q}{Re},\\A_{i+1}&=0.125A(\bar{u}_{i+1}+2\bar{u}_i)-\frac{\mu_{nf}}{\rho_{nf}LU_\infty}Q,\\A_{i-1}&=-0.125A\bar{u}_{i-1}-2\frac{\mu_{nf}}{\rho_{nf}LU_\infty}Q,\\A_{j+1}&=0.5B\bar{v}_j-\frac{\mu_{nf}}{\rho_{nf}LU_\infty}R,\\A_j&=3\frac{\mu_{nf}}{\rho_{nf}LU_\infty}R,\\A_{j-1}&=-0.5B\bar{v}_j-2\frac{\mu_{nf}}{\rho_{nf}LU_\infty}R.\end{aligned}\tag{40}$$

Novelty Journals

ISSN 2394-9651

International Journal of Novel Research in Physics Chemistry & Mathematics
Vol. 12, Issue 3, pp: (8-28), Month: September - December 2025, Available at: www.noveltyjournals.com

2) Y-Direction Momentum

Similarly the domain is subdivided along y-direction into regions on the left boundary with nodes $j = \overline{1,N}$, central region with nodes $j = \overline{N+1, MN-N+1}$ and upper $j = \overline{MN-M+1, NM}$, and are coupled with discretized momentum equations in the y-direction is formulated by considering the node $i = 1$ and $j = 1$, where the unknown values are $v_{1,1}$, $v_{2,1}$. For node $i = 1$ and $j = 10$, the unknown values are $v_{1,9}$, $v_{1,10}$. Letting the coefficient of $v_{1,9}$ be B_{27}, the coefficient of $v_{1,10}$ be B_{28}, and the known values on the right-hand side be f_{10}. Rewriting Equation (41) for node $i = 1$, $j = 10$, we extract terms corresponding to $v_{1,9}$ and $v_{1,10}$: Expanding the finite difference approximations:

$$\begin{aligned} &C[v_{k+1} - v_k] + 0.5A\bar{u}_{1,1}(v_{2,1} - v_{0,1}) + 0.125B\{v_{1,2}\bar{v}_{1,2} + 2v_{1,2}\bar{v}_{1,1} - 2\bar{v}_{1,0}v_{1,1} - \bar{v}_{1,0}v_{1,0}\} \\ &-\frac{1}{Re}\{Q(v_{2,1} - 3v_{1,1} + 2v_{0,1}) + R(v_{1,2} - 3v_{1,1} + 2v_{1,0})\} - \\ &D\frac{L}{U_\infty^2}\beta\rho_{nf}g(T_{1,1}\Delta T + T_\infty - T_r) = 0 \end{aligned} \tag{41}$$

Since this is a steady case of heat energy transfer, $C(v_{k+1} - v_k)$ term reduces to 0 and letting $\frac{\mu_{nf}}{\rho_{nf}LU_\infty} = \frac{1}{Re}$ and collecting like terms such that the unknown terms ($v_{1,1}$ and $v_{1,2}$) remain on the left hand side of the equation, yields;

$$\begin{aligned} &(-0.25B\bar{v}_{1,0} + \frac{3}{Re}(Q + R')v_{v_{1,1}} + (0.25B\bar{v}_{1,1} + 0.125B\bar{v}_{1,2} - \frac{R\prime}{Re})v_{1,2} = \\ &0.125B\bar{v}_{1,0}v_{1,0} - 0.5A\bar{u}_{1,1}v_{2,1} + 0.5A\bar{u}_{1,1}v_{0,1} + \frac{1}{Re}Q(v_{2,1} + 2v_{0,1}) \\ &+2\frac{R\prime}{Re}v_{1,0} + D\frac{L}{D_\infty^2}\rho_{nf}g(T_{1,1}\Delta T + T_\infty - T_r) \end{aligned} \tag{42}$$

Let the coefficient of $v_{1,1}$ be B_1, the coefficient of $v_{1,2}$ be B_2, the known values on the right hand side be f_1, yields equation

$$B_1 v_{1,1} + B_2 v_{1,2} = f_1. \tag{43}$$

Following the same procedures as in the case of x direction momentum, the system of equations can be expressed in matrix form as:

$$\begin{bmatrix} B_1 & B_2 & 0 & 0 & 0 & 0 & 0 & 0 & 0 & 0 \\ B_3 & B_4 & B_5 & 0 & 0 & 0 & 0 & 0 & 0 & 0 \\ 0 & B_6 & B_7 & B_8 & 0 & 0 & 0 & 0 & 0 & 0 \\ 0 & 0 & B_9 & B_{10} & B_{11} & 0 & 0 & 0 & 0 & 0 \\ 0 & 0 & 0 & B_{12} & B_{13} & B_{14} & 0 & 0 & 0 & 0 \\ 0 & 0 & 0 & 0 & B_{15} & B_{16} & B_{17} & 0 & 0 & 0 \\ 0 & 0 & 0 & 0 & 0 & B_{18} & B_{19} & B_{20} & 0 & 0 \\ 0 & 0 & 0 & 0 & 0 & 0 & B_{21} & B_{22} & B_{23} & 0 \\ 0 & 0 & 0 & 0 & 0 & 0 & 0 & B_{24} & B_{25} & B_{26} \\ 0 & 0 & 0 & 0 & 0 & 0 & 0 & 0 & B_{27} & B_{28} \end{bmatrix} \begin{bmatrix} v_1 \\ v_2 \\ v_3 \\ v_4 \\ v_5 \\ v_6 \\ v_7 \\ v_8 \\ v_9 \\ v_{10} \end{bmatrix} = \begin{bmatrix} f_1 \\ f_2 \\ f_3 \\ f_4 \\ f_5 \\ f_6 \\ f_7 \\ f_8 \\ f_9 \\ f_{10} \end{bmatrix} \tag{44}$$

where the coefficients are:

$$\begin{aligned} B_i &= 3\frac{\mu_{nf}Q}{\rho_{nf}LU_\infty}, \\ B_j &= 0.25(v_{j+1} - v_{j-1}) + \frac{3R\prime}{Re}, \\ B_{i+1} &= 0.5B\bar{v}_j - \frac{\mu_{nf}Q}{\rho_{nf}LU_\infty}, \\ B_{i-1} &= -0.5B\bar{v}_j - 2\frac{\mu_{nf}Q}{\rho_{nf}LU_\infty} \\ B_{j+1} &= 0.125B(\hat{v}_{j+1} + 0.25v_j) - \frac{R\prime}{Re} \\ B_{j-1} &= 0.125(2v_j - \hat{v}_j) - \frac{R\prime}{Re} \end{aligned} \tag{45}$$

Novelty Journals

ISSN 2394-9651

International Journal of Novel Research in Physics Chemistry & Mathematics
Vol. 12, Issue 3, pp: (8-28), Month: September - December 2025, Available at: www.noveltyjournals.com

This is upon imposing the necessary boundary conditions and initial guess for values of $\hat{u}$ and U in the solution domain. Equation (34) are coupled iteratively solved interchangeably until convergent solution for $\hat{v}$ and V be obtained with an acceptable tolerance $\epsilon = 0.0001$.

3) Energy Momentum

The two dimensional rectangular domain $\Omega \in \mathbb{R}^2$ divides region into segment, the heat equation results into a system of equation as a system of NM algebraic equations with NM unknowns hence from the known boundary conditions and substituting the approximate values of u and v obtained from Equation (34). The equations can be solved by Gaussian inversion of the discretized heat equation. The problem is therefore modelled as a linear steady direct heat storage problem in a rectangular transverse section of a thermally conducting Nano-fluid with no heat source, given by Eqns. (8) and (14) and simplified as follows

$$\begin{aligned} &\nabla^2 T = 0 \quad in \quad \Omega \quad \{0,1\} \quad \{0,d\} \\ &\frac{\partial T}{\partial n} = \varphi \quad on \quad \Gamma_1 = \{0,1\} \times \{0\} \\ &\frac{\partial T}{\partial n} = 0 \quad on \quad \Gamma_2 = \{0,1\} \times \{d\} \\ &\frac{\partial T}{\partial n} = 0 \quad on \quad \Gamma_2 = \{1\} \times \{0,d\} U \\ &\Gamma_4 = \{0\} \quad \times \quad \{0,d\}. \end{aligned} \tag{46}$$

When ϕ is a specified heat flux on the bottom side $y = 0$ and n is the outward unit normal to the boundary. Let N and M be number of control volume in the x and y axis respectively for a uniform discretization. Assuming that other heat flux and boundary temperatures are constant over each boundary segment $\Gamma_i = \{(x_{i-1}, y_{j-1}), (x_i, y_i)\}$ then the discretized heat equation at node i=1, j=1, unknown values are $T_{1,1}$ and $T_{2,1}$ becomes:

$$E_1 T_{1,1} + E_2 T_{2,1} = g_1 \tag{47}$$

$$E_3 T_{1,1} + E_4 T_{2,1} + E_5 T_{3,1} = g_2 \tag{48}$$

$$E_{27} T_{9,1} + E_{28} T_{10,1} = g_{10} \tag{49}$$

Resulting into NM unknown in the squared linear system of NM equations, allowing for straight forward inversion of the linear system of algebraic equation for the direct heat conduction problem (DHCP) which becomes

$$\sum_{j=1}^{N} A_{ij} T_j + \sum_{j=N+1}^{NM-N} A_{ij} T_j + \sum_{j=NM-N+1}^{NM} A_{ij} T_j = \sum_{j=1}^{N} B_{ij}, \qquad i = \overline{1,N} \tag{50}$$

We solve the linear system using the Gauss elimination Method. In case heat storage in the system occurs it is stored in terms of latent heat and temperature increases in the system of equation. We then solve the coupled system using Matlab, first by validating using a system of equations whose analytical solution is known in which are considered the steady state heat condition problem was considered and described by the Laplace equation is given by:

$$\nabla^2 T(x,y) = 0, (x,y) \in (0,1) \times (0,d), \tag{51}$$

and boundary condition

$$\begin{aligned} &-\frac{\partial T}{\partial n}, \quad (xy) \quad = \Pi \cos(\pi x) \qquad x, y \in \Gamma_1 = [0,1] \times \{0\} \\ &\frac{\partial T}{\partial n}(xy) \qquad = 0, \qquad (x,y) \in \Gamma_2 = 1 \times \{0,d\} \cup \Gamma_4 = \{0\} \times [0,d] \\ &\frac{\partial T}{\partial n}(xy) \qquad = g(T(x,y)), \qquad (x,y) \in \Gamma_3 = 1 \times \{0,1\} \times \{d\}, \end{aligned} \tag{52}$$

Novelty Journals

ISSN 2394-9651

International Journal of Novel Research in Physics Chemistry & Mathematics
Vol. 12, Issue 3, pp: (8-28), Month: September - December 2025, Available at: www.noveltyjournals.com

If $g(T) = -\pi T + \pi$ then the linear DHCP is an exact solution. $T(x, y) = \cos(\pi x)\exp(-\pi y) + 1$. This suggests a Laplace equation, which describes steady-state heat conduction (or similar physical processes) in a rectangular domain. The subsequent governing finite difference based on Eqn. (52) and suppose each coefficient E_i is derived based on the corresponding finite difference discretization:

- Convective terms: $0.5A\rho_{nf}(C_p)_{nf}u^*$ and $0.5B\rho_{nf}(C_p)_{nf}v^*$.
- Diffusive terms: $-\frac{k_{nf}}{U_\infty}Q$ and $-\frac{k_{nf}}{U_\infty}R$.
- Phase change terms: $S(H_{k+1} - H_k)$.

For a general finite difference node, the resulting coefficients can be written as:

$$E_i = \text{convection} + \text{diffusion} + \text{phasechange} \tag{53}$$

where convection terms appear as first-order derivatives in the x and y directions, diffusion terms appear as second-order derivatives in x and y and latent heat storage contributes through the enthalpy balance. The coefficients of equations generated from discretization of governing equations at different nodes in the control volume can then be converted into matrices then estimated for the purpose of investigation of heat transfer and storage in the PCM during charging process. The general discretized equation at at node $i = 1$ and $j = 1$ can be written as:

$$\begin{aligned} &S(H_{k+1} - H_k) + 0.5A\rho_{nf}(C_p)_{nf}u_{1,1}(T_{2,1} - T_{0,1}) \\ &+0.5B\rho_{nf}(C_p)_{nf}v_{1,1}(T_{(1,2)} - T_{1,0}) \\ &-\frac{k_{nf}}{U_\infty}\{Q(T_{2,1} - 3T_{1,1} + 2T_{0,1}) + R(T_{1,2} - 3T_{1,1} + 2T_{1,0})\} = 0 \end{aligned} \tag{54}$$

Grouping all terms in the form $A\mathbf{T} = \mathbf{g}$, results in coefficient matrix for a system of equations:

$$\begin{bmatrix} E_1 & E_2 & 0 & 0 & 0 & 0 & 0 & 0 & 0 & 0 \\ E_3 & E_4 & E_5 & 0 & 0 & 0 & 0 & 0 & 0 & 0 \\ 0 & E_6 & E_7 & E_8 & 0 & 0 & 0 & 0 & 0 & 0 \\ 0 & 0 & E_9 & E_{10} & E_{11} & 0 & 0 & 0 & 0 & 0 \\ 0 & 0 & 0 & E_{12} & E_{13} & E_{14} & 0 & 0 & 0 & 0 \\ 0 & 0 & 0 & 0 & E_{15} & E_{16} & E_{17} & 0 & 0 & 0 \\ 0 & 0 & 0 & 0 & 0 & E_{18} & E_{19} & E_{20} & 0 & 0 \\ 0 & 0 & 0 & 0 & 0 & 0 & E_{21} & E_{22} & E_{23} & 0 \\ 0 & 0 & 0 & 0 & 0 & 0 & 0 & E_{24} & E_{25} & E_{26} \\ 0 & 0 & 0 & 0 & 0 & 0 & 0 & 0 & E_{27} & E_{28} \end{bmatrix} \begin{bmatrix} T_1 \\ T_2 \\ T_3 \\ T_4 \\ T_5 \\ T_6 \\ T_7 \\ T_8 \\ T_9 \\ T_{10} \end{bmatrix} = \begin{bmatrix} g_1 \\ g_2 \\ g_3 \\ g_4 \\ g_5 \\ g_6 \\ g_7 \\ g_8 \\ g_9 \\ g_{10} \end{bmatrix} \tag{55}$$

where the coefficients are:

$$\begin{aligned} E_i &= 0.5B\rho_{nf}(Cp)_{nf} + \frac{3k_{nf}}{U_\infty}(Q + R) \\ E_{i-1} &= -0.5A\rho_{nf}(C_p)_{nf}\bar{u}_{i,1} - \frac{2k_{nf}}{U_\infty}Q, \\ E_{i+1} &= 0.5A\rho_{nf}(C_p)_{nf}\bar{u}_{i,1,1} - \frac{k_{nf}}{U_\infty}Q. \end{aligned} \tag{56}$$

The matrix in Eqn. (55) is formed to allow solving for the temperature field T numerically.

Novelty Journals

ISSN 2394-9651

International Journal of Novel Research in Physics Chemistry & Mathematics
Vol. 12, Issue 3, pp: (8-28), Month: September - December 2025, Available at: www.noveltyjournals.com

IV. RESULTS AND DISCUSSION

A. Parameter Estimation

The numerical simulations depends on the following parameters estimated in Table 2.

Table 2: Parameter estimation (Estimation is based on Aluminum Oxide (Al_2O_3) as nano particles) and PCM

Parameter	Description	Value range	Value used	Value Computed	Units	Source
ρ_p	Density of Al_2O_3	$4-4.95$	4.5		$3*g/cm^3$	[10]
$2*\rho_{PCM}$	Density of $NaNO_3$	2.26	-	2*2.17		[8]
	Density of KNO_3	2.11				[9]
Cp	Heat capacity of Al_2O_3	$0.849-0.9$	0.88	-	$3*J/K$	[3]
$2*Cp_{PCM}$	Heat capacity of $NaNO_3$	$0.072-0.298$	0.129	2*0.137		[2]
	Heat capacity of KNO_3	0.142	-			[7]
β_p	Coefficient of Thermal expansion volume of Al_2O_3	75×10^{-6}	-	75×10^{-6}	$3*/K$	[14]
$2*\beta_{PCM}$	Coefficient of Thermal expansion volume of $NaNO_3$	83×10^{-6}	-	2*57.2		[5]
	Coefficient of Thermal expansion volume of KNO_3	$30-100\times10^{-6}$	40			[6]
k_P	Thermal conductivity of Al_2O_3	237	-	-	$3*W/mK$	[18]
$2*k_{PCM}$	Thermal conductivity of $NaNO_3$	$0.5-0.512$	0.512	2*0.58		[11]
	Thermal conductivity of KNO_3	0.62	-			[15]

B. Validation of the Momentum and Boundary Equations

1) X-Direction

Equations (34) is simulated based on Equation (46) and results presented in Figure 6.

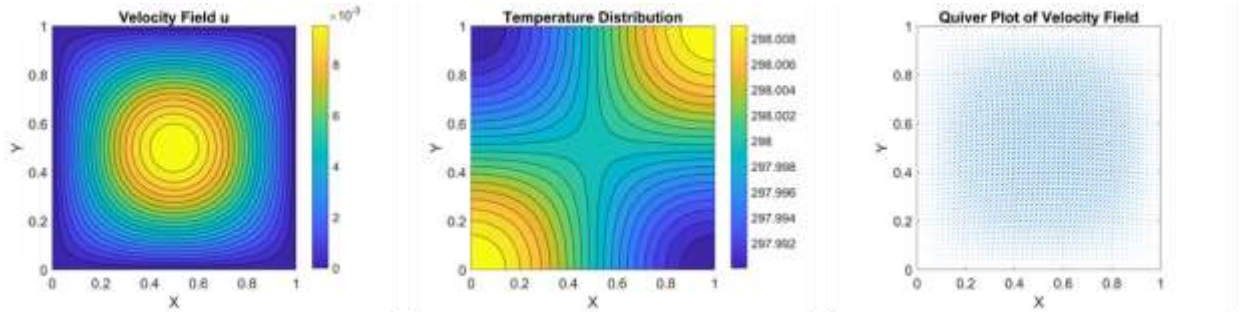

Figure 6: Simulation of velocity and temperature based on momentum equation in the x direction using Equation (34).

The simulation results in Figures 6 illustrate the velocity and temperature fields within a NaNO $_3$–Al $_2$O $_3$ NePCM cavity, revealing the dominant role of natural convection driven by temperature-dependent buoyancy forces. The quiver plot shows a well-organized recirculating flow characterized by a strong upward motion along the vertical centreline, where the highest temperature gradients occur. This behaviour reflects classical buoyancy-driven convection, governed by the term $-\beta g(T-T_r)$ in the momentum equation. Near the boundaries, velocity magnitudes decrease due to no-slip effects and partially solid regions of PCM. The filled velocity-magnitude contours confirm a symmetric, stable convection cell

Novelty Journals

ISSN 2394-9651

International Journal of Novel Research in Physics Chemistry & Mathematics
Vol. 12, Issue 3, pp: (8-28), Month: September - December 2025, Available at: www.noveltyjournals.com

accurately resolved by the tridiagonal discretisation. The temperature distribution mirrors the flow structure, with a clear gradient from the hotter upper-right region to the cooler lower-left, indicating strong thermal–fluid coupling. Nanoparticle enhancement increases thermal conductivity, intensifies convection, and produces more uniform energy distribution. The simulations capture the essential mechanisms of melting, heat transport, and fluid motion in NePCM systems.

2) Y-Direction

Equation (37) is simulated and results presented in Figure 7.

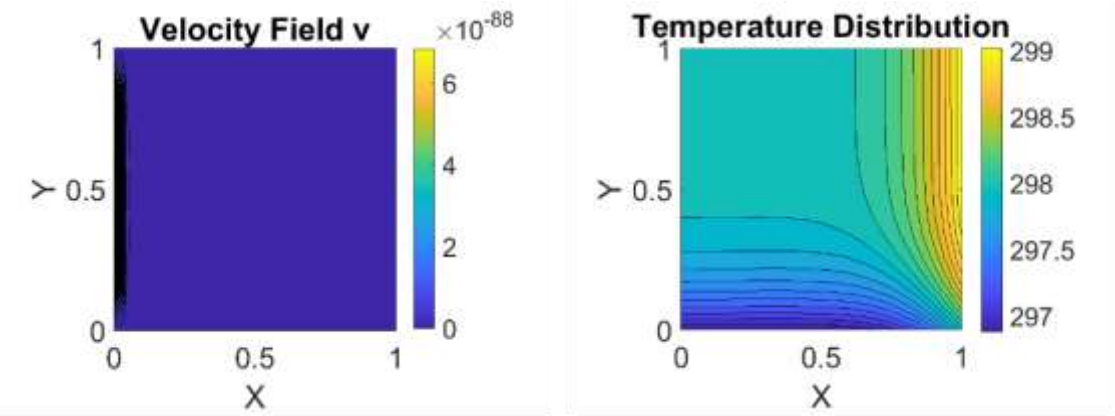

Figure 7: Simulation of velocity and temperature based on momentum equation in the y direction using Equation (37).

Figure 7 shows the simulated velocity and temperature fields in the y-direction, revealing highly localized convective motion near the left boundary and negligible velocities across the rest of the domain. This indicates that natural convection is weak and that heat transfer is dominated by thermal conduction rather than fluid motion. The limited velocity variation suggests suppressed convective transport, with thermal diffusion enhanced by nanoparticles becoming the primary mechanism of heat redistribution. The temperature field exhibits a strong gradient along the right boundary, forming a well-defined thermal boundary layer and indicating asymmetric melting concentrated near the heat source. The absence of strong convection promotes thermal stratification but improves conductive heat diffusion. Comparing Figures 6 and 7, the x-direction shows a strong buoyancy-driven recirculation cell, whereas the y-direction flow remains confined and minimal. This contrast confirms that NePCM behaviour is governed by dominant vertical convection and weak horizontal motion, while temperature distributions remain largely similar in both directions.

3) Energy

Validity of boundary condition in Equation (46) is presented in simulation shown in Figure 8.

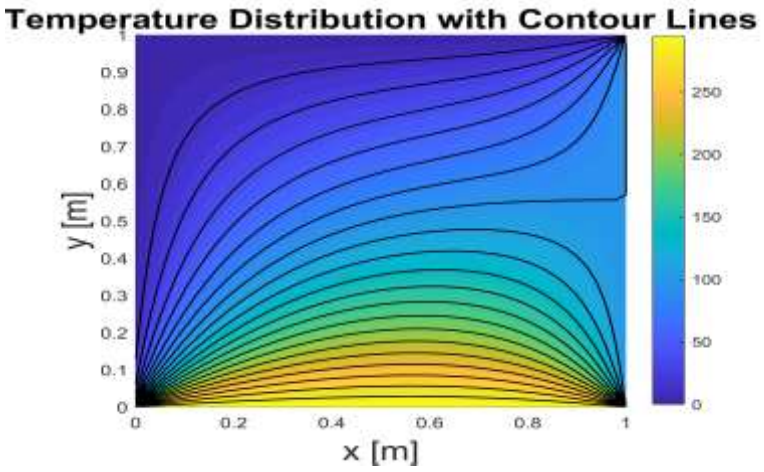

Figure 8: Validation of the boundary conditions presented in Equation (46).

Novelty Journals

ISSN 2394-9651

International Journal of Novel Research in Physics Chemistry & Mathematics
Vol. 12, Issue 3, pp: (8-28), Month: September - December 2025, Available at: www.noveltyjournals.com

Figure 8 shows the temperature field obtained after repositioning the thermal boundary conditions, with the bottom boundary now acting as the heat source. The highest temperatures appear along the lower surface, and the dense contour clustering indicates a steep gradient and strong upward heat flux driven by the imposed Neumann condition $\frac{\partial T}{\partial n} = -\phi$. The top boundary displays cooler, uniformly distributed temperatures, consistent with the insulated condition $\frac{\partial T}{\partial n} = 0$. The left and right vertical boundaries remain nearly isothermal, confirming minimal lateral heat diffusion under adiabatic constraints. The overall pattern demonstrates stable, upward conductive heat transfer from the heated bottom toward the insulated top. The smooth progression of contours and the absence of numerical artefacts verify that the applied boundary conditions are correctly implemented and that the conduction model performs reliably within the defined thermal configuration.

C. Validation of Velocity, Momentum and Energy Distribution

1) Y Direction

Equation (39) is simulated based on the optimal values in Table 2 and the results presented in Figure 9.

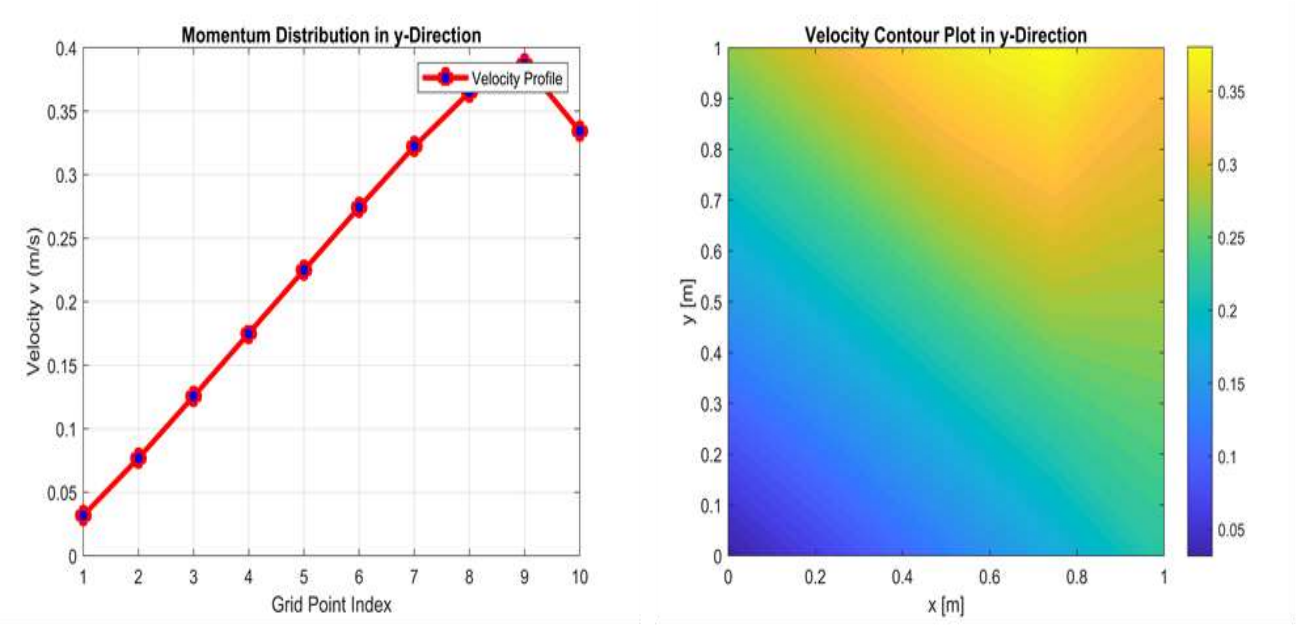

Figure 9: Simulation showing the velocity profile and intensity for momentum equation in y direction at different nodes.

Figure 9 presents the momentum and velocity distribution in the y-direction, showing how natural convection influences molten NePCM flow. The velocity profile exhibits an upward increase from the bottom to the top grid index, indicating buoyancy-driven motion as heated, low-density fluid rises. The red curve and blue FVM markers align closely, confirming numerical consistency and a stable linear velocity progression. The accompanying contour map further illustrates this behaviour, with low velocities near the bottom and higher velocities toward the upper region, demonstrating a transition from conduction-dominated to convection-dominated zones. The addition of nanoparticles enhances thermal conductivity, reduces temperature gradients, and strengthens convective currents, leading to greater velocity magnitudes. Nanoparticles also modify viscosity, influencing the intensity of momentum transport. Overall, the results show that enhanced convection in the y-direction accelerates heat distribution, reduces charging and discharging time, improves fluid mixing, and minimizes thermal stratification, thereby supporting efficient and durable PCM thermal-energy storage performance.

Novelty Journals

ISSN 2394-9651

International Journal of Novel Research in Physics Chemistry & Mathematics
Vol. 12, Issue 3, pp: (8-28), Month: September - December 2025, Available at: www.noveltyjournals.com

2) X Direction

The matrix in Equation (39) is simulated based on the optimal values in Table 2 to obtain the results in Figure 10.

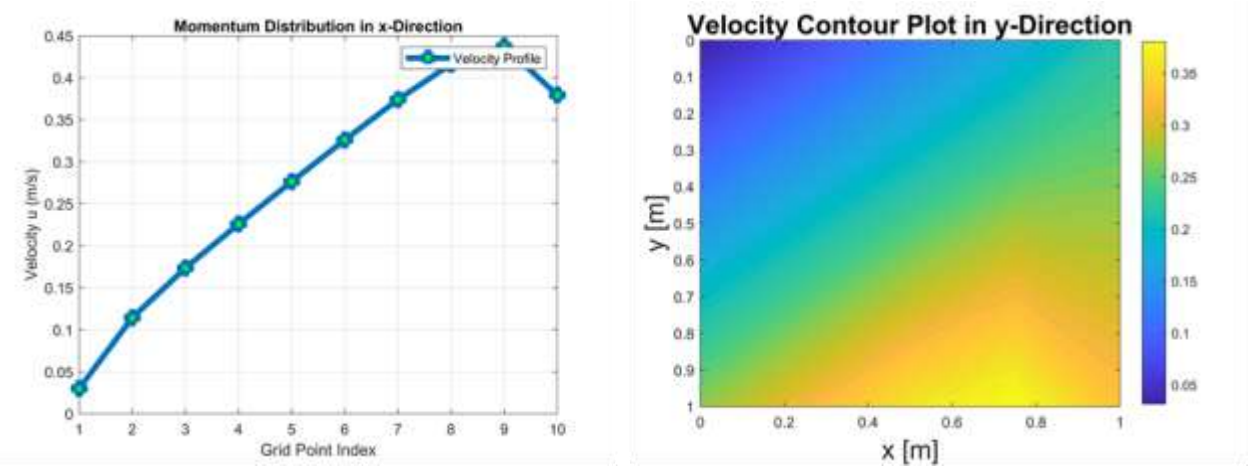

Figure 10: Simulation showing the velocity profile and intensity for momentum equation in x direction at different nodes.

Figure 10 illustrates the velocity and momentum behaviour in the x-direction, confirming that nano-enhanced PCMs significantly strengthen convective heat transfer by increasing thermal conductivity and reducing thermal resistance. The velocity contour reveals a smooth gradient from low velocities in the lower-left region to higher velocities in the upper-right, indicating stable convective motion essential for efficient heat distribution in TES systems. The uniformity of the field and the absence of abrupt variations demonstrate balanced momentum transport and reduced thermal stratification. The line plot shows a progressively increasing momentum profile, driven by enhanced conduction and improved buoyancy effects due to nanoparticle dispersion. Peak velocities occurring near the upper grid points signify the region of strongest convective activity, followed by a slight decline associated with boundary-layer stabilization toward the domain edges. This behaviour aligns with expected fluid-flow dynamics in confined thermal systems. The results confirm that NePCM improves both conduction and convection, supporting faster heat transfer and more efficient phase-change cycling in thermal energy storage applications.

3) Energy

The matrix (55) is solved numerically in order to allow the visibility of the temperature field T as presented in Figure 11.

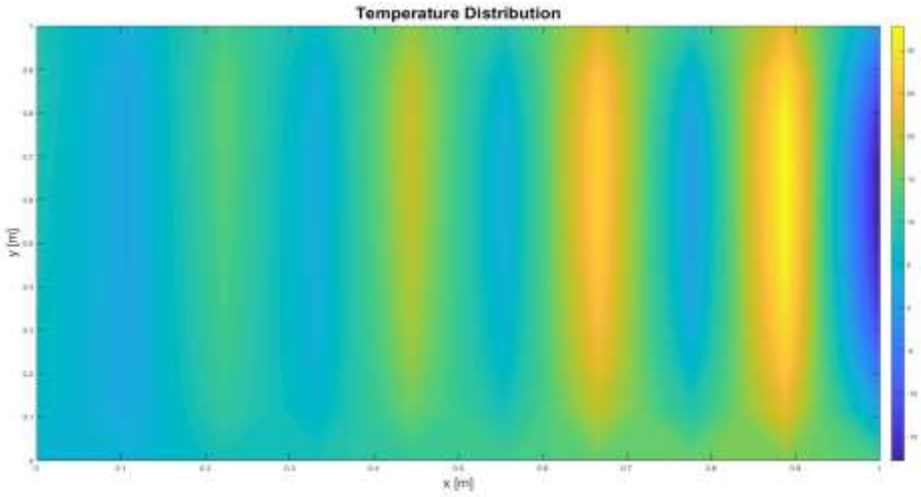

Figure 11: Simulation showing the energy at different nodes based on Equation (55).

Figure 11 shows the temperature distribution plot illustrates the thermal behavior of the nano-PCM during the storage process. The color gradient in the plot, transitioning from blue to yellow, represents the temperature variation. The presence of alternating high and low-temperature bands suggests the development of convection currents within the PCM. The formation of these convection cells indicates the influence of buoyancy-driven flow, where hotter, less dense fluid rises while cooler, denser fluid sinks. This circulatory motion significantly enhances heat transfer efficiency compared to purely conductive heat transport. The reduction of thermal stratification due to nano-enhancement ensures a more uniform temperature profile, preventing localized overheating or undercooling.

D. Discussion

The results of this study show that formulation of boundary conditions play a decisive role for the accuracy, stability and physical realism of finite volume simulation of Nano-Enhanced Phase Change Materials (NePCMs). The velocity fields from the discretised x- and y-direction momentum equation agree very well with empirical and numerical literature. The x direction simulations have a well-developed buoyancy driven convection cell, with the maximum velocity magnitudes concentrated at the centre of the cavity. This behaviour is consistent with that of NePCMs which led to a faster melting and better thermal homogenization studied by [16] although this study did not test the effect of boundary conditions. The present results are a step forward in their observations in that they show that the strength and structure of convective flow is extremely sensitive to the type and formulation of boundary conditions used.

Similarly, the temperature distribution verifies increased thermal diffusion from the addition of nanoparticles in accordance with conduction–convection mechanisms from [4]. However, although the present study also uses Hosseini's work as a basis on the geometric optimisation of fins, the present study explains that the boundary conditions themselves have a strong effect on the distribution of heat flux and melt-front evolution. The numerical results verify that the Neumann heat flux boundaries at the heated base and the adiabatic boundaries along the vertical direction give us a physically realistic temperature gradient as can be seen by the smooth contour distribution and agreements with the analytical Laplacian Solutions.

The y-direction momentum results further show a directionally-dependence of the strengths of convection with the y-direction being dominated by weak velocity fields. This supports the observations of [1], who identified improper treatment of boundaries can suppress or exaggerate the flow in PCM systems. The present study confirms that the application of correct normal gradient boundary conditions eliminates spurious oscillations and assures the stability of the velocity and temperature fields.

Additionally, the energy-distribution simulation shows decreases in thermal stratification and spread of temperature when boundary conditions are adequately formulated. This outcome is very much in agreement with the results of [12] who showed that NePCM simulations are extremely sensitive to the numerical stability constraints without taking into account the boundary effects. The stability, convergence behaviour and physical accuracy of NePCM heat transfer predictions are significantly improved by the present results obtained by boundary-condition modelling.

Overall, the discussion creates an understanding that the boundary conditions are not peripheral numerical inputs but central modelling parameters that control the strength of the convection, continuity of heat flux, motion of interface, numerical stability. This study therefore addresses a crucial methodological gap by presenting a validated transferable framework for the formulation of boundary conditions in NePCM finite volume modelling.

V. CONCLUSION

The increased interest in Phase Change Materials (PCMs) and Nano-Enhanced PCMs (NePCMs) are due to the increased global demand of efficient thermal energy storage systems because of their capabilities of offering features including uniform energy distribution, high thermal conductivity and faster melting/solidification cycles. Despite the fact that NePCM research has made significant progress, one important methodic problem of NePCM research has been not solved; the proper formulation and the validation of the boundary conditions in finite volume simulations. Prior studies often assumed generic boundary conditions and this contributed to numerical instability, poor tracking of the melt front as well as poor predictive reliability. This study was therefore undertaken to meet this gap in the methodology.

The research determined the full framework of boundry conditions of NePCM modelling with Neumann boundray Condition, Dirichlet boundary condition and mixed boundry condition with the finite volume technique. By working with the discretised momentum and energy equations using the nanoparticle enhanced thermophysical properties and inversion schemes the study of the velocity and temperature fields under representative boundary settings were simulated. The results found that the specification of boundary conditions have major effects on the convection strength of and the continuity of heat flux, as well as the patterns of the velocity field, and also on the global stability of the simulations. Physically realistic behaviours such as buoyancy-driven convection, conduction governed boundary layers and uniform thermal gradients were triggered for appropriately implemented and verified boundary conditions.

The conclusion of the study is that the formulation of the boundary condition is a fundamental aspect in the order to ensure accurate modelling of NePCMs, and ultimately determines the stability and the predictive power of the modelling of numerical simulations. The results thus constitute a validated and transferable structure of the modelling of thermal storage systems based on NePCM and to a large degree.

Recommendations for policy and future research include the inclusion of validated boundary condition frameworks into thermal energy systems modelling standards, incentive for industry application of NePCMs for robust use of numerical modelling, expansion of the present framework to transient three dimensional configurations, inclusion of experimental validation of boundary effects, and the development of adaptive boundary algorithms as part ofdynamic thermal environments.

REFERENCES

[1] D. Chiappini, “A coupled lattice Boltzmann–finite volume method for phase change material analysis,” *International Journal of Thermal Sciences*, vol. 164, p. 106893, 2021.

[2] O. Enea, P. P. Singh, E. M. Woolley, K. G. McCurdy, and L. G. Hepler, “Heat capacities of aqueous nitric acid, sodium nitrate, and potassium nitrate at 298.15 K: δC°p of ionization of water,” *The Journal of Chemical Thermodynamics*, vol. 9, no. 8, pp. 731–734, 1977.

[3] T. K. Engel, “The heat capacities of Al_2O_3, UO_2 and PuO_2 from 300 to 1100 K,” *Journal of Nuclear Materials*, vol. 31, no. 2, pp. 211–214, 1969.

[4] M. M. Hosseini and A. B. Rahimi, “Heat transfer enhancement in solidification process by change of fins arrangements in a heat exchanger containing phase-change materials,” *International Journal of Numerical Methods for Heat & Fluid Flow*, 2018.

[5] M. Md Ibrahim, V. Ramachandran, K. Sarangapani, and R. Srinivasan, “Thermal expansion of sodium nitrate (I),” *Journal of Physics and Chemistry of Solids*, vol. 47, no. 5, pp. 517–520, 1986.

[6] M. Ji, L. Lv, J. Liu, Y. Rong, and H. Zhou, “$NaNO_3$–KNO_3/EG/Al_2O_3 shape-stable phase change materials for thermal energy storage over a wide temperature range: Sintering temperature study,” *Solar Energy*, vol. 258, pp. 325–338, 2023.

[7] M. Kawakami, K. Suzuki, S. Yokoyama, and T. Takenaka, “Heat capacity measurement of molten $NaNO_3$–$NaNO_2$–KNO_3 by drop calorimetry,” in *VII International Conference on Molten Slags Fluxes and Salts*, The South African Institute of Mining and Metallurgy, pp. 201–208, 2004.

[8] M. A. Kedzierski, “Viscosity and density of aluminum oxide nanolubricant,” *International Journal of Refrigeration*, vol. 36, no. 4, pp. 1333–1340, 2013.

[9] W. Laue, M. Thiemann, E. Scheibler, and K. W. Wiegand, “Nitrates and nitrites,” *Ullmann’s Encyclopedia of Industrial Chemistry*, 2000.

[10] M. Liu, P. Masset, and A. Gray-Weale, “Solubility of sodium in sodium chloride: A density functional theory molecular dynamics study,” *Journal of The Electrochemical Society*, vol. 161, no. 8, p. E3042, 2014.

[11] R. Li, J. Zhu, W. Zhou, X. Cheng, and Y. Li, “Thermal properties of sodium nitrate-expanded vermiculite form-stable composite phase change materials,” *Materials & Design*, vol. 104, pp. 190–196, 2016.

[12] F. A. Misawo, T. T. Onyango, and F. O. Nyamwala, "Analyzing stability of nano-enhanced PCM via control volume method," *International Journal of Novel Research in Physics Chemistry & Mathematics*, vol. 12, no. 1, pp. 86–103, 2025.

[13] F. A. Misawo, T. T. Onyango, and F. O. Nyamwala, "A control volume analysis of energy distribution on nano-enhanced phase change material," *International Journal of Recent Research in Interdisciplinary Sciences (IJRRIS)*, vol. 12, no. 2, pp. 1–10, 2025.

[14] H.-Y. Peng et al., "Terahertz characterization of functional composite material based on ABS mixed with ceramic powder," *Optical Materials Express*, vol. 13, no. 9, pp. 2622–2632, 2023.

[15] M. Roshandell, *Thermal Conductivity Enhancement of High Temperature Phase Change Materials for Concentrating Solar Power Plant Applications*, PhD Thesis, UC Riverside, 2013.

[16] S. K. Sahoo, M. K. Das, and P. Rath, "Numerical study of cyclic melting and solidification of nano enhanced phase change material based heat sink in thermal management of electronic components," in *ASME 5th International Conference on Micro/Nanoscale Heat and Mass Transfer*, pp. 1–8, 2016.

[17] M. Vinokur, "An analysis of finite-difference and finite-volume formulations of conservation laws," *Journal of Computational Physics*, vol. 81, no. 1, pp. 1–52, 1989.

[18] A. Zhang and Y. Li, "Thermal conductivity of aluminum alloys—A review," *Materials*, vol. 16, no. 8, p. 2972, 2023.